Lanthanide-based complexes as efficient physiological temperature sensors

Bernardo Monteiro[a], João Paulo Leal[a,b], Ricardo F. Mendes[c], Filipe A. Almeida Paz[c], Anthony Linden[d], Volodymyr Smetana[e], Anja V. Mudring[e], João Avó*[f], Cláudia C. L. Pereira*[g]

[a] Centro de Química Estrutural (CQE), Departamento de Engenharia Química (DEQ), Instituto Superior Técnico, Universidade de Lisboa, Campus Tecnológico e Nuclear, Estrada Nacional 10, 2695-066 Bobadela, Portugal.

[b] Centro de Química Estrutural (CQE), DECN, Instituto Superior Técnico, Universidade de Lisboa, Campus Tecnológico e Nuclear, Estrada Nacional 10, 2695-066 Bobadela, Portugal.

[c] CICECO—Aveiro Institute of Materials, Department of Chemistry, University of Aveiro, 3810-193 Aveiro, Portugal.

[d] Department of Chemistry, University of Zurich, Winterthurerstrasse 190, CH-8057, Zurich, Switzerland

[e] Department of Materials and Environmental Chemistry, Stockholm University, Svante Arrhenius väg 16 C, 10691 Stockholm, Sweden

[f] Institute for Bioengineering and Biosciences (IBB) and Associate Laboratory i4HB—Institute for Health and Bioeconomy, Instituto Superior Técnico, Universidade de Lisboa, Av. Rovisco Pais, 1049-001 Lisboa, Portugal.

[g] LAQV-REQUIMTE, Departamento de Química, Faculdade de Ciências e Tecnologia, Universidade Nova de Lisboa, 2829-516 Caparica, Portugal.

Abstract:

A new molecular thermometric sensor based on the terbium(III) complex $[C_2mim][Tb(fod)_4]$ (C_2mim – 1-methyl-3-ethylimidazolium, fod^- - tetrakis-6,6,7,7,8,8,8-heptafluoro-2,2-dimethyl-3,5-octanedionate), doped with 0.015% of its europium(III) analogue (**1**, $[C_2mim][Tb(fod)_4]_{0.99985}$:$[C_2mim][Eu(fod)_4]_{0.00015}$), was prepared and its thermochromic behaviour evaluated from ambient temperature up to 75 ºC, including in the physiological range (35-45 °C). It was found that the intensity ratio of the $^5D_4 \rightarrow {}^7F_5$ (Tb^{III}) and $^5D_0 \rightarrow {}^7F_2$ (Eu^{III}) transitions is correlated with temperature having three different linear regimes. Visual colorimetry allowed the evaluation of the temperature in different ranges from green at ambient temperature, to yellow and finally red at higher temperatures. The Tb^{III} complex emission intensity is extremely sensitive to small temperature variations, particularly between 25 and 35 ºC, were it reaches only 40% of the initial intensity.

Confinement of the dopped Tb^{III} tetrakis-complex in the organic polymeric matrix poly(methylmethacrylate) (PMMA) induced higher thermal stability in **1**, together with a strong temperature dependence of the most intense emissive transition of the Tb^{III} complexes. The photoluminescence quantum yield of polymer-lanthanide hybrid materials increased significantly compared with that of **1**. Under 366 nm irradiation, the hybrid material presents a green colour at 25 ºC that evolves to yellow at 30 ºC and to a white tone at 35 ºC.

Introduction

Contactless thermometers are extremely important in research fields such as microelectronics and nanomedicine. Hyperthermia, a recently developed therapeutic method for the treatment of cancer diseases, uses localized heat on tumorous lesions at temperatures between 40-45 ºC for 60-90 minutes.[1] Temperature monitoring is important for reducing the risk of thermal toxicity due to excessive heating, higher than 43.5 ºC, the temperature at which healthy cells start to die. A recent study recommends the usage of at least fifty sensors for adequate evaluation of tissue temperature during frequent treatments.[2]

Thermometry based on the luminescence of lanthanides (Ln) relies mostly on the measurement of the intensity of two distinct emitting centers, using more effectively the ratio of the most intense transitions of Tb^{III} and Eu^{III}, $^5D_4 \rightarrow {}^7F_5$ and $^5D_0 \rightarrow {}^7F_2$, respectively. Usually, these Tb^{III}/Eu^{III} combinations have the best performances at very low temperatures, *ca.* -70 ºC, rendering them less adequate for biological applications.

Luminescent thermal probes based exclusively on the emissive properties of terbium are rare. Incorporation of $Eu(tfa)_3/Tb(tfa)_3$ complexes in a 1:1 metal ratio in a phenanthroline-polymer yielded a material with yellow emission colour.[3] Recently, Brito and co-workers published the trivalent tetrakis complexes $[C_4mim][Tb_{1-x}Eu_x(btfa)_4]$ (btfa- - 4,4,4-trifluoro-1-phenyl-2,4-butanedionate) with a temperature dependence of the intensity ratio between the most intense bands: $^5D_4 \rightarrow {}^7F_5$ from Tb^{III} and $^5D_0 \rightarrow {}^7F_2$ from Eu^{III}, with relative thermal sensitivity around 7.6% at -253.15 ºC and a minimum temperature uncertainty below 0.03 ºC.[4] Interestingly, using the excitation wavelength at 360 nm, attributed to the chromophore ligand singlet-singlet transition ($S_0 \rightarrow S_1$), the thermometer works in the -253 to -73 ºC range. Shifting the excitation wavelength to 489

nm, which corresponds to the direct excitation of Tb^{III}, the operating interval is -123 to -48 ºC with a maximum sensitivity (S_m) higher that 1%.

An unusual and rarely reported behaviour was observed for an Eu/Tb mixed MOF [$Eu_{0.01}Tb_{0.99}NDC$] (NDC^{2-} = 1,4-naphthalenedicarboxylate) at the physiological temperature range, after optimization of the used organic ligand by using information about its energy triplet level.[5] In this case, the fluorescence intensity of Tb^{III} decreases slowly, while Eu^{III} quenches rapidly. As a consequence, the self-referencing thermometric parameter Δ($\Delta = I_{Tb}/I_{Eu}$) increases exponentially, being more pronounced in the 120-200 ºC range. Other lanthanide MOF thermometers working in the physiological range are Eu^{III}/Tb^{III} halides post-functionalized in a MIL type MOF of In.[6] The thermal sensitivity of $I_{Eu}.I_{Tb}$@In-MOF-253 is 4.97% $ºC^{-1}$. A NIR luminescent MOF with Nd^{III} and Yb^{III} ions using a highly symmetric ligand, [$Nd_{0.95}Yb_{0.05}BPTC$], BPTC - 1,10-biphenyl-3,30,5,50-tetracarboxylate, presented exponential-type luminescence responses to temperatures between 19.8-49.8 ºC with a maximum sensitivity of 0.94% C^{-1} at the lower temperature.[7] Ananias et al. reported the influence of the Tb^{III} concentration on the tetragonal lanthanide triad silicate $Na[(Gd_xTb_yEu_z)SiO_4]\cdot nNaOH$ nanothermometer working at cryogenic temperatures with a remarkable maximum sensitivity of 6.2% C^{-1} at -261 ºC.[8]

Carlos and co-workers explored the use of Covalent Organic Frameworks (COFs) as supports for the preparation of hybrid materials as ratiometric luminescent temperature sensors. Interestingly, for the Eu/Tb systems, there is no thermal quenching of the Tb^{III} emission because of the absence of ion-to-ligand/host energy back transfer, a behaviour rarely observed in Ln^{III} based materials.[9]

In most cases, temperature sensitivity of lanthanide materials works by means of temperature quenching because of the deactivation of the luminescent excited states of

lanthanide ions.[10] For a detailed explanation of the temperature sensitive mechanisms, the authors suggest a recently published review article where the standardization of luminescence thermometry for biomedical applications is discussed.[11]

The present work stems from our interest in designing luminescent thermal probes for semi-contact temperature sensors based on lanthanide tetrakis-β-diketonate complexes. Uncommon thermochromic features of the $[Eu(fod)_4]^-$ complex anion (fod^- - tetrakis-6,6,7,7,8,8,8-heptafluoro-2,2-dimethyl-3,5-octanedionate) were recently reported by us.[12]

For an effective energy transfer process in Eu^{III} and Tb^{III}, the T_1 energy level of the ligands should be higher than the $^5D_0$ and $^5D_4$ level of Eu^{III} and Tb^{III} (17200 and 20400 cm^{-1}, respectively). Generally, Tb^{III} complexes are more prone to back energy transfer processes than Eu^{III}, because the donor level of the ligand is located at 3250 cm^{-1}.[13] The triplet energy state of the fod^- sensitizer is 22500 cm^{-1}, only 2080 cm^{-1} above the emitting level $^5D_4$ of Tb^{III} (Scheme 1).

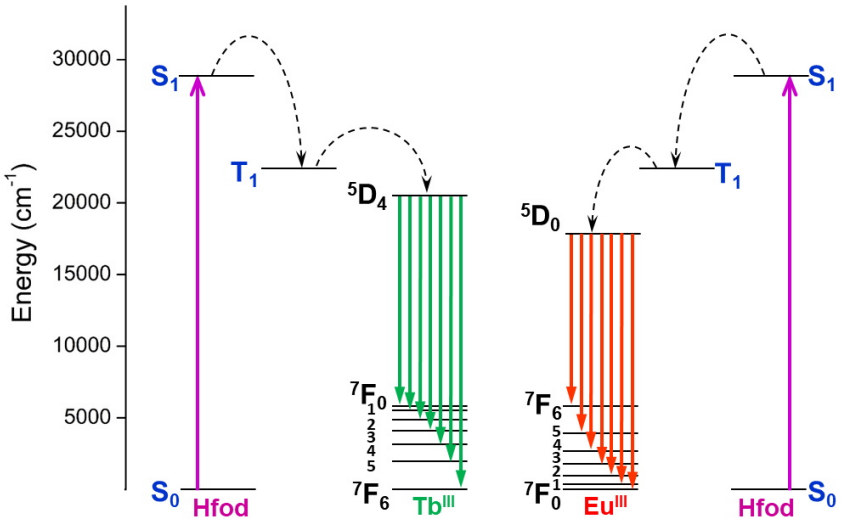

Scheme 1. Energy level diagram for the transfer processes of $[C_2mim][Tb(fod)_4]_{1-x}[C_2mim][Eu(fod)_4]_x$.

The observed thermochromism originating from an unusual, and apparently diketone-exclusive, anion-cation interaction through the fod^- ligand was detected for the $[C_2mim][Tb(fod)_4]$ complex at temperatures between 25 and 40 ºC. This ratio was found because of ratiometic relationships between different bands from the $^5D_4 \rightarrow {}^7F_5$ transition, which change their relative intensity upon increasing the temperature. This subject will be discussed at the end of the following section.

More interestingly, the ratio between I($^5D_4 \rightarrow {}^7F_5$) from Tb^{III} and the Eu^{III} I($^5D_0 \rightarrow {}^7F_2$) transition bands, showed a ratiometric thermal behaviour at physiological temperatures when an extremely low amount of the Eu^{III} complex is used in the Tb^{III}/Eu^{III} mixture.

The effect of fluorination on the optical properties of lanthanide β-diketonates has been the subject of intensive research and it was concluded that $-CF_3$ groups are responsible for a significant increase in the emission intensity when compared with the $-CH_3$ analogue.[14] Besides having higher luminescent intensities and being thermally more stable, highly fluorinated β-diketone lanthanide complexes show suppression of non-radiative decay paths because of the low frequency of the C–F vibrational oscillators.[15] Moreover, the effect of fluorination on the absolute quantum yield for Eu^{III} luminescence was reported for $[Eu(fod)_3dpbt]$ as being 59%, which is higher than the 45% found for $[Eu(tta)_3dpbt]$.[16]

Doping lanthanide complexes in polymer matrices allows easier manipulation, increased thermal resistance and higher photostability. Poly(methylmethacrylate) (PMMA) is a popular host matrix because of its transparency at wavelengths higher than 250 nm. Here, we report the thermometric behaviour of $[C_2mim][Tb(fod)_4]_{0.99985}$:$[C_2mim][Eu(fod)_4]_{0.00015}$ (**1**) embedded in a PMMA matrix with a loading of 10% (w/w). A remarkable change of temperature-dependent emission was

observed under a UV lamp (excitation wavelength 366 nm), with green emission at 25 ºC evolving to yellow at 30 ºC and a white tone at 35 ºC. At temperatures higher than 50 ºC an orange/pink colour is observed, mainly arising from the Eu^{III}-complex emission.

Results and Discussion

Thermal behaviour and room temperature luminescence

Thermal stress resistance of **1** was investigated by thermogravimetric analysis (TGA) between 25 and 600 ºC (Figure 1a) under an air atmosphere at rates of 10 ºC min^{-1}.

The TGA profiles of **1** revealed a remarkable thermal stability with decomposition not setting in until around 200 °C, with only 2% weight loss, which is expected for highly fluorinated complexes that have very low amounts of adsorbed water or retained solvent. Full decomposition comprises the formation of oxyfluorides of terbium and europium, which represent 17.4% of the initial mass.

As observed in other complexes of the $[Eu(fod)_4]^-$ family, an endothermic solid–solid phase transition occurs in **1** with an endothermic peak with T_{on} at 99.5 ºC for the heating, and an exothermic peak at 77.9 °C for the cooling (Figure 1b). Analysis of the DSC profile shows a reversible change between two solid phases (a case of polymorphism). The ΔH value was readily calculated from the area of the DSC curve (both the cooling and heating). The difference between the transition temperature in the cooling and heating curves arises from some inertia of the process and can be associated with a small barrier to be overcome in the transformation from one phase to the other. One of the possibilities for overcoming this barrier is to use the entropy increase associated with the increase of temperature. It is therefore possible to calculate for the phase transition, considering the value of the enthalpy (ΔH=+29.78 kJ mol^{-1}), an entropy associated with the process of transformation (ΔS=+78.36 J mol^{-1} K^{-1}), as well as estimate a small activation energy of

2.28 kJ mol^{-1}. The nature of the phase transformation that occurs between the two solid phases cannot be deduced solely from the analysis of the DSC. However, it can be explained if it is associated with a solid-solid phase transition, frequently reported for some organic ionic liquids based on the C_2mim^+ cation, but uncommonly described for inorganic compounds.[17,18]

The profile of the calorimetric analysis (DSC) is apparently independent of the lanthanide centre and the nature of the cation. We have repeatedly observed a thermal process between 80 and 100 ºC, attributed to a reversible solid-solid phase transition, reflected in the colour of the complex, which changes from light yellow to deep purple at temperatures close to 100 ºC. The causes behind this phenomenon are not yet fully understood, although evidence indicates that a strong interaction between fluorinated chains of fod^- and the cation is promoted by an increase of temperature.[12]

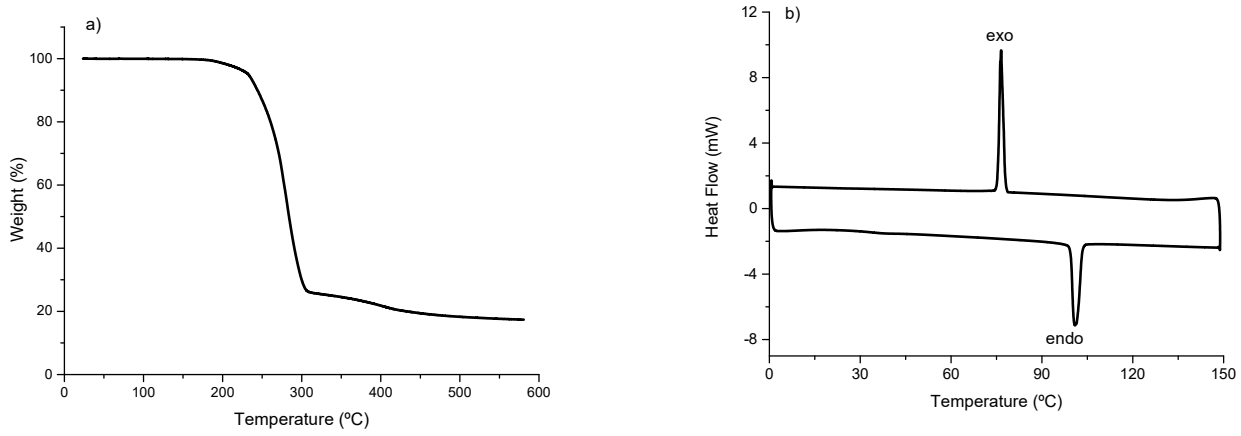

Figure 1 a) TGA profile of **1**. b) DSC curve of **1** recorded with a heating rate of 5 °C min^{-1} from 20 to 150 °C.

Important parameters for Eu^{III} and Tb^{III} complexes to be used as biological probes in biological media are large Stokes shifts, narrow emission bands and long excited-state

lifetimes (ms).[19,20] Complex **1** shows strong luminescence at ambient temperature, attributed to the non-aromatic character of the β-diketonate ligand, thereby ensuring that the energy of the triplet level (T_1) is higher than those of the resonance level $^5D_4$ of Tb^{III} and $^5D_0$ of Eu^{III}.[21]

The full emission spectra centred on the most intense $^5D_4 \rightarrow {}^7F_5$ transition of the Tb^{III} cation at 545 nm, recorded at ambient temperature, is depicted in Figure 2. When excited at 350 nm, the emission of $[C_2mim][Tb(fod)_4]$ exhibits narrow emission lines in the range of 400-650 nm, corresponding to the $^5D_4 \rightarrow {}^7F_{3,4,5,6}$ transitions of Tb^{III}. At the same excitation wavelength for $[C_2mim][Eu(fod)_4]$, the $^5D_0 \rightarrow {}^7F_1$ (590 nm) and $^5D_0 \rightarrow {}^7F_2$ (612 nm) transitions are less predominant, while the low intensity $^5D_0 \rightarrow {}^7F_0$ (579 nm) band is hidden by the $^5D_4 \rightarrow {}^7F_4$ Tb^{III} transition.

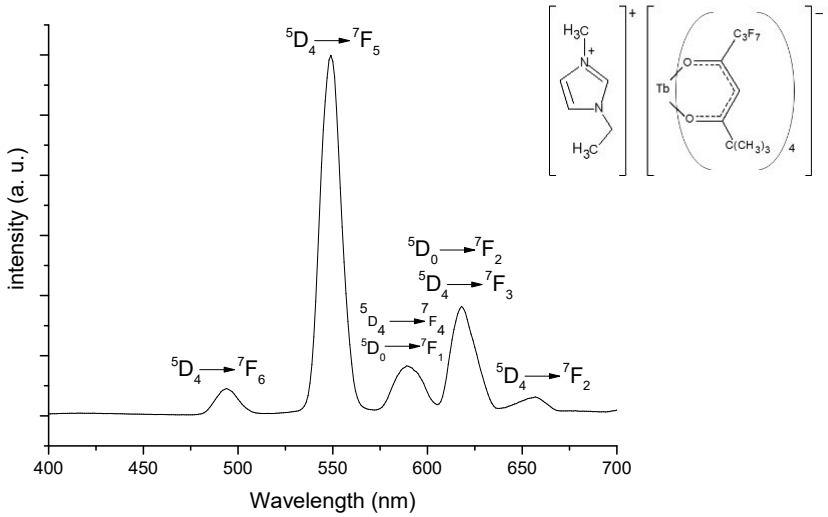

Figure 2 Full emission spectra of $[C_2mim][Tb(fod)_4]_{0.99985}$:$[C_2mim][Eu(fod)_4]_{0.00015}$ (**1**) at ambient temperature upon excitation at 350 nm. Inset: the $[C_2mim][Tb(fod)_4]$ structure.

In the sensitization process, the light energy is absorbed by the ligand in a singlet-singlet transition and then intersystem crossing decay populates a lower lying triplet state (T_1) that transfers energy, non-radiatively, to the resonant 4*f* level of the Ln^{III} ion, which

subsequently emits at characteristic wavelengths.[22] According to a theoretical rule developed for europium and terbium complexes, efficient energy transfer occurs when the energy difference between the first excited triplet state of ligands (T_1) and the resonant level of the Ln^{III} ion is around 2500–3500 cm^{-1}.

The phenomenon of energy back-transfer from the Ln^{III} ions to the ligand, which reduces the luminescence intensity, is induced by a temperature increase, frequently reaching very low emission intensities at temperatures close to that of the ambient. As presented below, this effect was much more pronounced for $[C_2mim][Tb(fod)_4]$ than for $[C_2mim][Eu(fod)_4]$.

Temperature-sensitive luminescence assays of 1 and 1@PMMA

Figure 3a shows the excitation spectrum of **1** monitored around the more intense 545 nm emission line for the Tb^{III} ion. A broadening and shift in the excitation band maximum was observed from a single band at 25 ºC (340 nm), to broader bands with a maximum of 370 nm at 75 ºC. A red shift for the maximum excitation intensity is probably related to the peculiar and unusual effect of temperature on the coordination mode of fod^- to the lanthanide centre.[12] As expected, the ligand absorption band is dominant because of the well-known forbidden Ln^{III} *f-f* electronic transitions and the very low extinction coefficients. This band corresponds to the $S_0 \rightarrow S_1$ singlet-single transition from the fod^- ligand and $[C_2mim]$ cation.[4]

The ambient temperature spectra derived from absorption and diffuse reflectance measurements of **1** in the UV-visible region (300-500 nm) is depicted in Figure 3b. The

broad and intense absorption band in the 300-350 nm range is associated with the π-π* intra-ligand transition of the fod^- ligand from the S_0 ground state to the S_1 excited state.[23]

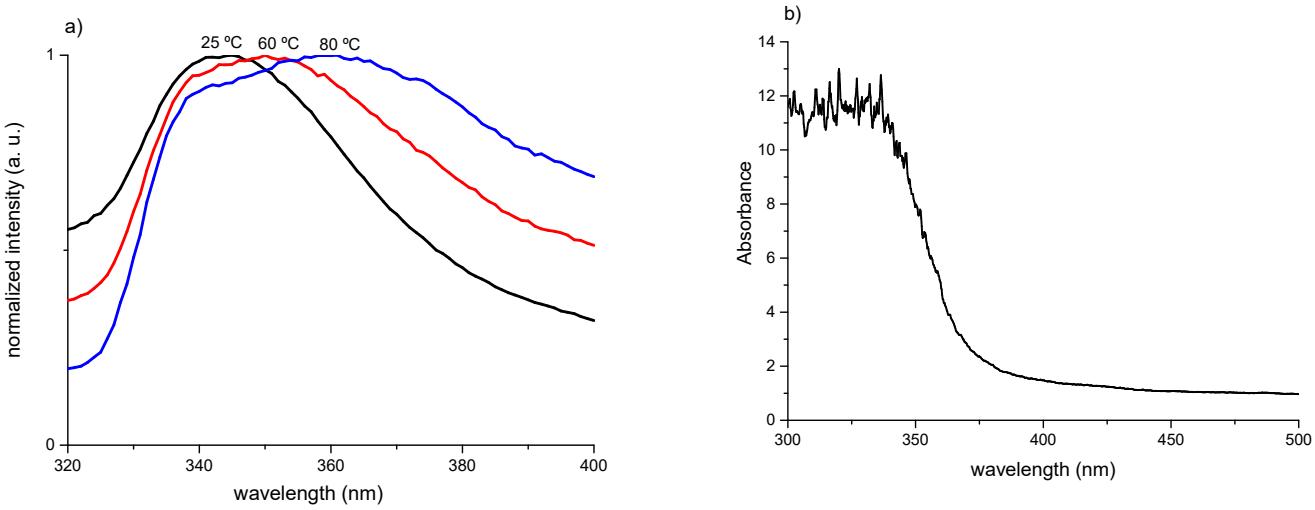

Figure 3 a) Normalized excitation spectra monitored for the $^5D_4 \rightarrow {}^7F_5$ transition of Tb^{III} at different temperatures. b) Absorption spectrum of **1**.

The photophysical properties and unusual temperature dependence of $[C_2mim][Eu(fod)_4]$ were discussed in detail in our previous work and were not considered relevant for the observed thermochromism of $[C_2mim][Tb(fod)_4]_{0.99985}$:$[C_2mim][Eu(fod)_4]_{0.00015}$.[24]

The solid-state emission spectra of **1** were recorded between 450 and 650 nm, under excitation of the ligand absorption band at 350 nm, from 25 to 75 ºC with 1 ºC steps between 35 and 45 ºC. Upon heating, the fluorescence intensity of Tb^{III} decreases dramatically, while that of Eu^{III} decreases at a much slower rate. The emission intensity decreases by around 40% from 25 to 30 ºC and by up to 60% at 35 ºC. This is an uncommon behaviour, not usually observed in other Tb^{III} complexes, that allows the observed high thermometric sensitivity at temperatures close to ambient temperature and slightly higher, including physiological temperatures, up to 75 ºC where it reaches only 10% of the initial emission intensity (Figure 4).

In a similar fashion, for the dinuclear complex of Tb^{III} containing the ligand 1,8-bis(2-hydroxy-benzamido)-3,6-dioxaoctane, a reduction of emission intensity of close to 50% was observed between 20 ºC and 60 ºC, along with a sensitivity of the luminescent intensity of 1.13% C^{-1}.[26] The effect is probably observed because of the deactivation of the $^5D_4$ state of the Tb^{III} cation, mainly through the back-energy transfer from the $^5D_4$ state to the triplet excited state of the antenna chromophore of the ligand.[25,26] In this case, a close match between the energy of the T_1 state and the energy of the Tb^{III} 4*f* level (Scheme 1) significantly influences the back-transfer mechanism. The position of the T_1 level is very temperature dependent, so the luminescence promoted by the 'antenna effect' of the chromophore can be perturbed by a temperature increase.

Besides the well-known reported quenching effect of temperature, attributed to the thermal population of the triplet state of the fod^- ligand by the emitting $^5D_4$ state [27], in this case, the decrease of the emission intensity may have some contribution from a relevant influence of the temperature on the coordination environment around the terbium centre, to which corresponds a lower energy transference from the ligand to the metal centre, as will be discussed below.

Assuming the optical properties of $[C_2mim][Eu(fod)_4]$,[24] the option of using an extremely low ratio of Eu/Tb stems from the fact that a highly emissive Eu^{III} complex could hide the Tb^{III} signal. Despite the intense green luminescence, the intrinsic quantum yield (Φ) of the Tb^{III} complex is only 2% and is surprisingly low compared with other Tb^{III} diketonate complexes[13,28] or its Eu^{III} analogue, which presents a value for Φ_{Eu} of 82%. Quantum efficiency values close to 5% were, however, found for the highly fluorinated tris-diketonate Tb^{III} complex, $Tb(hfa)_3bpm$.[29]

Under the employed Tb/Eu concentration ratio there is a spectral overlap between the $^5D_4 \rightarrow {}^7F_3$ and the $^5D_0 \rightarrow {}^7F_2$ red emissions of Tb^{III} and Eu^{III}, respectively. For the presented

results, the superposition is not relevant because we have used relative intensities instead of total area of the considered emission bands (Figure 4).

24

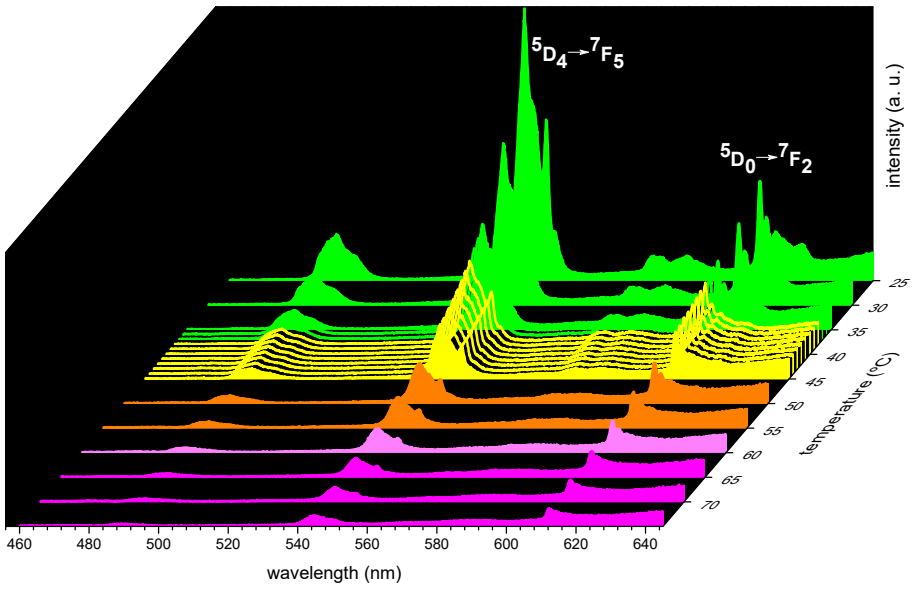

Figure 4 The evolution of the emission spectra of $[C_2mim][Tb(fod)_4]_{0.99985}$:$[C_2mim][Eu(fod)_4]_{0.00015}$ upon excitation at a wavelength of 350 nm, selectively exciting Tb^{III}. Yellow lines represent emission at physiological temperatures measured with 1 ºC steps between 35 and 45 ºC.

Three different linear ratiometric relationships were found (Figure 5) with a drastic decrease between 25 and 36 ºC, which is associated with a very high absolute sensitivity of 10% C^{-1}. From 37 to 60 ºC, where the experimental temperature increment was 1 ºC in the 35-45 ºC range, linearity between I_{545}/I_{612} and temperature was found, although with a lower absolute sensitivity of 3%.

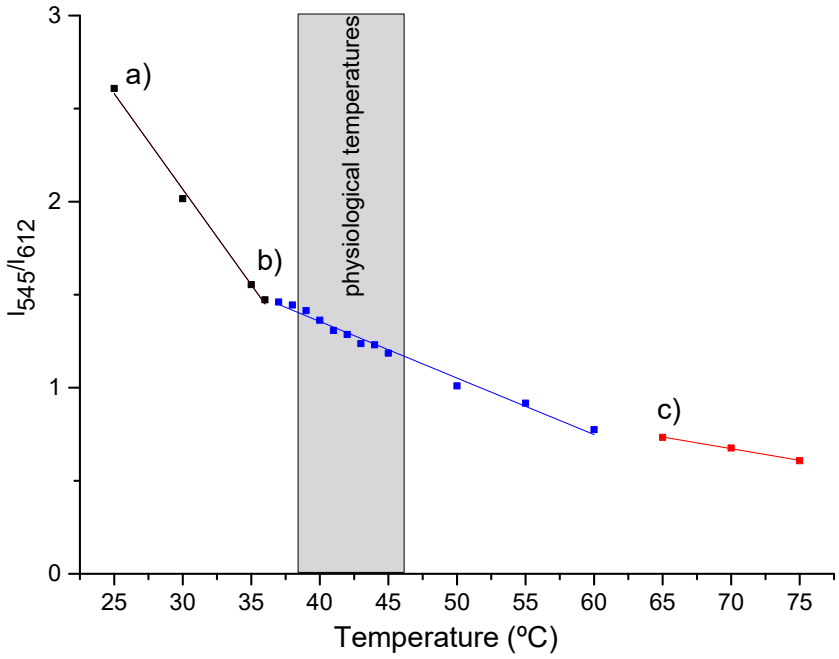

Figure 5 The solid lines show the best linear fit for I_{545}/I_{612}. a) 25-36 ºC Δ=-0.10T + 5.14 (r^2=0.992), b) 37-60 ºC Δ=-0.030T + 2.57 (r^2=0.987), c) 65-75 ºC Δ= -0.012T + 1.55 (r^2=0.994).

The emission intensity of the $^5D_0 \rightarrow {}^7F_2$ transition from Eu^{III} starts to decrease very discreetly only at temperatures close to 35 ºC, while that from Tb^{III} is significantly reduced with each heating step. These two interesting features allow the deduction of a ratiometric relationship at biological temperatures with considerable maximum relative sensitivity (S_r, %) of 4.1% at 41 ºC. At temperatures above 65 ºC, $^5D_4 \rightarrow {}^7F_5$ and $^5D_0 \rightarrow {}^7F_2$ transition bands have low intensity, although at this stage $I(^5D_0 \rightarrow {}^7F_2)$ is slightly higher than $I(^5D_4 \rightarrow {}^7F_5)$. The final colour of the $[C_2mim][Tb(fod)_4]_{0.99985}$:$[C_2mim][Eu(fod)_4]_{0.00015}$ homogeneous mixture when heated to 100 ºC is pink.

The Commission Internationale de L'éclairage (CIE) chromaticity diagram of **1** was calculated at different temperatures from the corresponding corrected emission spectra

(Figure 6). Under 350 nm excitation, the emission colour changes from light green at 25 ºC, to yellow at 35 ºC and finally becomes bright red at 75 ºC. The tetrachromatic (light green, yellow, orange, and red) series reflects the balance between the $^5D_4 \rightarrow {}^7F_5$ and $^5D_0 \rightarrow {}^7F_2$ transition intensities in all ratiometric temperature sensing studies based on these lanthanides.

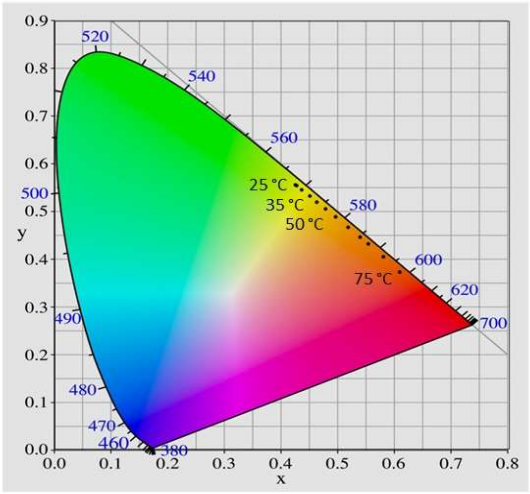

Figure 6 CIE chromaticity coordinate changes of **1** at different temperatures under λ_{exc}=340 nm.

The relative thermal sensitivity (Sr, %) is an important parameter that reflects the performance of the thermometer. Δ is the measured temperature sensitive parameter I_{545}/I_{612}, $\boldsymbol{\partial}$T is the estimate of the temperature uncertainty (1 ºC) and $\boldsymbol{\partial}\Delta$ is the variation in Δ.[30]

$$Sr = \frac{1}{\Delta}\frac{\partial \Delta}{\partial T} \qquad (1)$$

In the physiological temperature range, the relative sensitivity has the lowest value of 0.8% at 37 ºC, increasing up to the maximum value of 4.1% at 41 ºC. Values close to 4% were found at 43 ºC and 45 ºC (Figure 7).

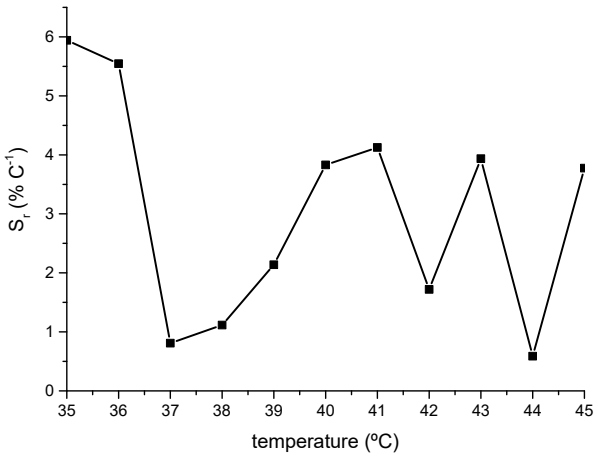

Figure 7 Relative thermal sensitivity (S_r %) in the physiological temperature range.

The thermochromic performance of **1** was run in triplicate with the same sample after total recovery of initial emission properties. The I_{545}/I_{612} versus temperature graph profile (Figure 5) was reproducible across three consecutive repetitions.

Table 1 Comparison of the sensitivity of recently reported ratiometric sensing probes working at physiological temperatures. Materials, the temperature range of analysis range (ΔT), and maximum relative sensitivity (S_m% C^{-1}) under the temperature range.

Material	ΔT(ºC)	S_m (% C^{-1})	Ref.
Phen-polymer@Eu,Tb_tfac	-13.1-186.8	2.34	[3]
$Eu_{0.01}Tb_{0.99}NDC$	20-60	7.32	[5]
$Na_2([Eu_{0.53}Tb_{0.47}(tfac)_8]_2$	6.8-106.8	2.70	[31]
$[Tb(H_5btp)].2H_2O$	25.8-45.8	1.43	[32]
PMMA[TbEuLtppo]	-20-39.8	4.21	[33]
$Tb_{0.08}Eu_{0.02}Gd_{0.9}(Carb)_3.H_2O$	24-45	5.32	[34]
$Tb_{0.9}Eu_{0.1}$Phenim	29.8-149.8	1.75	[35]
$[C_2mim][Tb(fod)_4]_{0.99985}.[C_2mim][Eu(fod)_4]_{0.00015}$	**36-45**	**4.1**	**This work**

As already stated, both the quantum efficiency and the decay time depend on the level of energy transfer of the donor (fod^-) to the acceptor, and on the emitting energy levels of the lanthanide ions, which in turn depend on the distance between the acceptor and donor energy levels.[36]

The $^5D_4 \rightarrow {}^7F_4$ transition (λ_{em}=545 nm) lifetimes of **1** were acquired and fitted with a bi-exponential decay curve ($\tau_{Total} = A + B_1\exp(-t/\tau_1) + B_2\exp(-t/\tau_2)$), indicating that the Tb^{III} dye undergoes a complex deactivation pathway with two components (Figure 8a, Table 2). The longest component (*ca.* 0.3 ms at 5 °C) is typical for Tb^{III} metal centers in the absence of relevant non-radiative deactivation processes.[37] Thus, the short component is attributed to the energy back-transfer from Tb^{III} centers to surrounding ligands. Upon heating, both components undergo a decrease in lifetime, and the short component becomes prevalent, leading to a marked decrease in overall emission lifetime (Figure 8b). These results suggest that temperature promotes the deactivation through energy back-transfer, which is more prevalent in Tb^{III} centres than Eu^{III} complexes, giving rise to the observed ratiometric thermal sensitivity of our system.

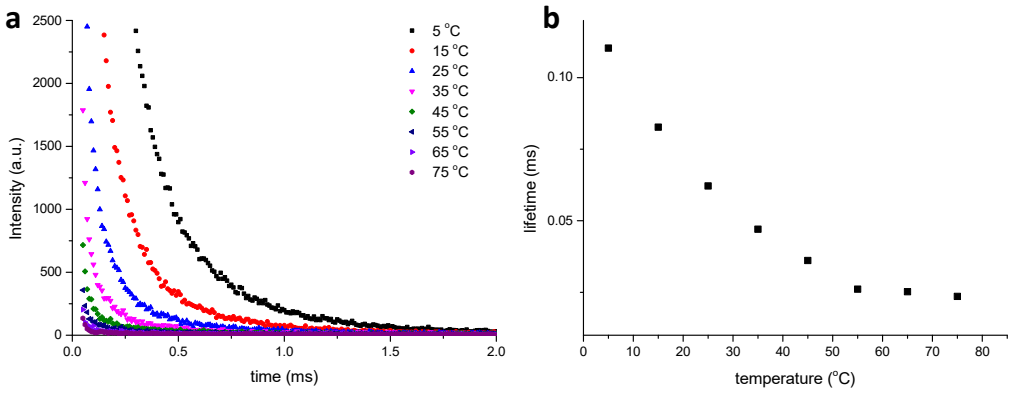

Figure 8 Lifetime measurements of Tb^{III} complex from 5 to 75 °C measured at 545 nm corresponding to the $^5D_4 \rightarrow {}^7F_4$ transition (λ_{exc}=350 nm).

Table 2 Observed luminescence lifetime ($\tau_{obs.}$, ms) and amplitudes (B) of **1** from 5 ºC to 75 ºC.

T (ºC)	τ_1 (ms)	τ_2 (ms)	B_1	B_2	τ_m (ms)
5	0.055	0.312	0.24	0.42	0.110
15	0.041	0.281	0.18	0.32	0.083
25	0.031	0.238	0.13	0.24	0.032
35	0.024	0.211	0.10	0.16	0.047
45	0.020	0.181	0.14	0.16	0.036
55	0.020	0.159	0.11	0.10	0.026
65	0.020	0.153	0.16	0.14	0.025
75	0.020	0.145	0.08	0.031	0.023

We have previously observed for a polysulfone (PSU) membrane, hosting 10 % (w/w) of $[C_2mim][Eu(fod)_4]$, a linear decrease of the $I(^5D_0\rightarrow{}^7F_2)/I(^5D_0\rightarrow{}^7F_1)$ ratio in the range 110 -150 ºC.[24]

Poly(methylmethacrylate), known as acrylic glass owing to its transparency and chemical stability, presents some advantages over other organic polymers, including protection from water, high transparency, good optical properties and improved photostability under UV irradiation of the guest complexes.

After embedding **1** in PMMA (10% w/w), the wavelength of the maximum emission increased from 545 nm to 550 nm for the $^5D_4\rightarrow{}^7F_5$ transition of the Tb^{III} complex and from 612 nm to 619 nm for the $^5D_0\rightarrow{}^7F_2$ transition of $[C_2mim][Eu(fod)_4]$. The emission spectra are dominated by these two transitions and the spectra resemble the host $[C_2mim][Tb(fod)_4]_{0.99985}$:$[C_2mim][Eu(fod)_4]_{0.00015}$ (Figure 4).

The excitation spectra were monitored for both the $^5D_4 \rightarrow {}^7F_5$ and $^5D_0 \rightarrow {}^7F_2$ transitions of **1**@PMMA at 25 and 75 ºC and are depicted in Figure S1 (Supporting Information).

The temperature-dependent emission spectra of the functionalized material, **1**@PMMA, are illustrated in Figure 8a and show a gradual decrease of intensity of the $^5D_4 \rightarrow {}^7F_5$ transition band from Tb^{III}, responsible for the green emission of the material at 25 ºC. Because of thermal activation of nonradiative deactivation pathways, induced by the temperature increase, the luminescence intensity of Tb^{III} decreases dramatically as the temperature increases from 25 to 100 ºC, while that of Eu^{III} decreases at a much slower rate. Upon heating, the green component decreases, while the intensity of the red contribution from Eu^{III} remains almost constant up to 45 ºC, at which temperature the balance of emissions results in **1**@PMMA emitting a light-yellow colour under 350 nm excitation wavelength (Figure 9a).

Ratiometric luminescent thermometry was also found in 1@PMMA with a temperature dependent ratio I_{550}/I_{612} that can be fitted with the polynomial relation; $\Delta = 5.27 - 0.11T + 6.0 \times 10^{-4} T^2$ and r^2 of 0.998 (Figure 9b).

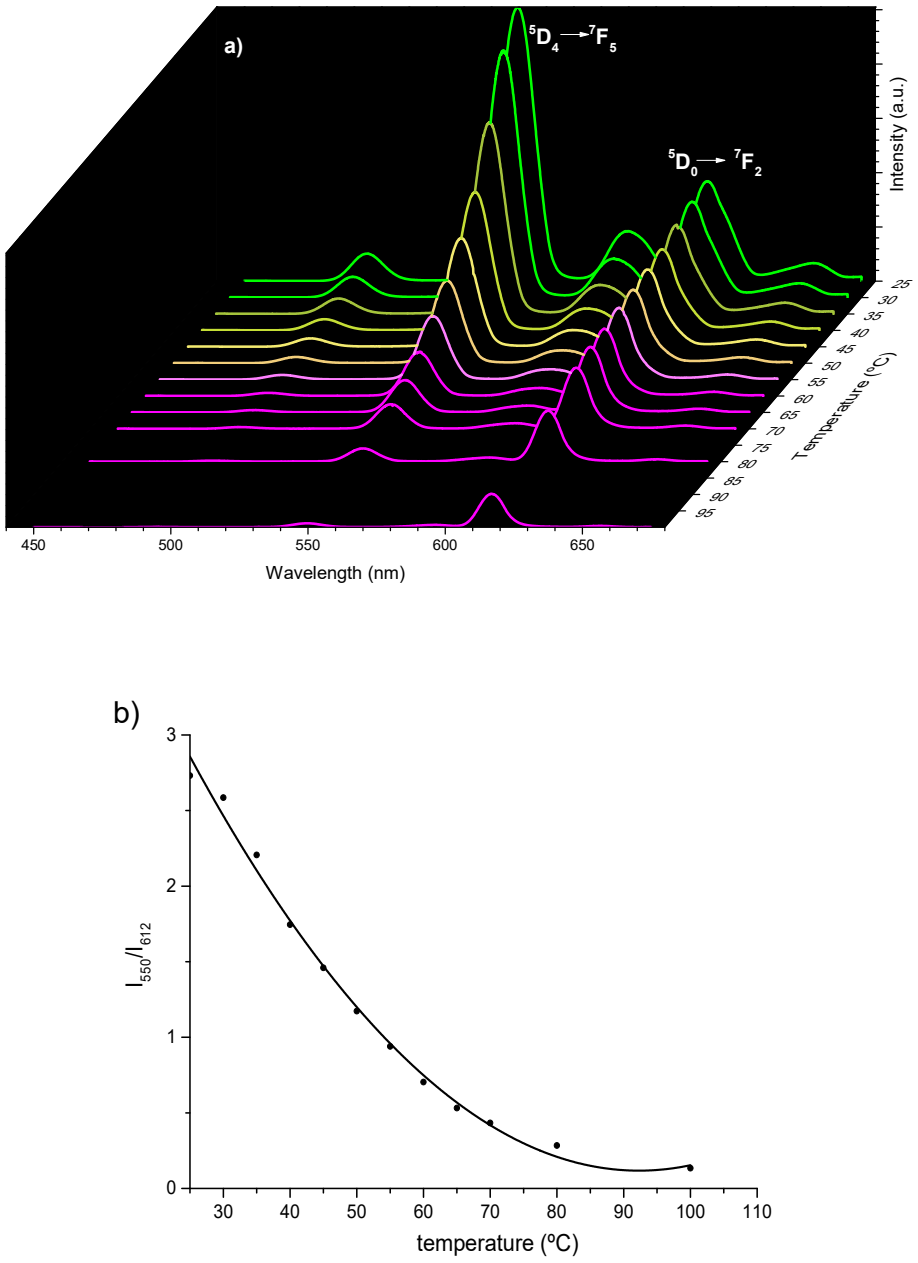

Figure 9 a) Emission spectra of **1**@PMMA recorded between 25 and 100 ºC by using an excitation wavelength of 350 nm. b) Temperature dependent ratio I_{550}/I_{612} with polynomial fit found $\Delta=5.27 -0.11T + 6.0x10^{-4}T^2$ and r^2 of 0.998.

Under 366 nm UV-lamp irradiation, the emission colours can easily be tuned by discrete variations of temperature. A small variation of only 5 ºC, from 25 to 30 ºC, allows the functionalized material to change from emitting green to emitting yellow and then a white tone at only 35 ºC. Finally, at temperatures higher than 55 ºC the red emission from Eu^{III} dominates the spectra with 30% of the initial emission intensity at 100 ºC (Figure 9a).

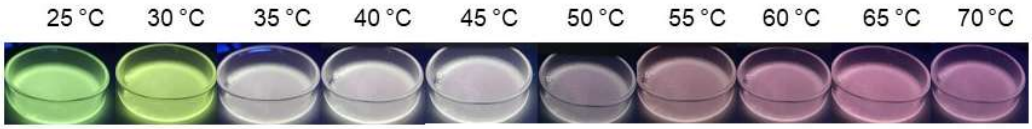

Figure 10 Pictures of **1**@PMMA material deposited on the top surface of glass under 366 nm irradiation at different temperatures.

The intrinsic quantum yield (Φ) of **1** increased more than two-fold when embedded in PMMA: from 2% in the pure solid to 5.1% when immobilized in the polymeric matrix. Improvement of Φ of the luminescent lanthanide complexes was previously reported after confinement in PMMA.[38,39] According to one of these studies, PMMA affects the coordination environment of the Tb^{III} ions and changes the energy transfer probabilities of the electric dipole transitions, which are reflected in a higher relative intensity of the $^5D_4 \rightarrow {}^5F_5$ transition.[39]

This organic/inorganic hybrid material foresees interesting applications in photovoltaics (PV) as luminescent solar concentrators (LSC).[40] Depending on the outside temperature to which the photovoltaic device is exposed, complementary absorption of the full solar spectrum can be achieved, reducing the mismatch between the AM1.5G spectrum and the PV cells absorption (Figure 10).

The morphology of the polymer matrix PMMA and the as-prepared films were inspected by Surface Scanning Electron Micrograph (SEM). The SEM images show that PMMA particles have a regular size (Figure 11a) and **1**@PMMA particles, after removal of the

film deposited onto the glass surface, have an approximate size of 200 μm (Figure 11b). PMMA films have inherent brittleness and after complex incorporation, the solid presented crystal shape particles with very small micropores.

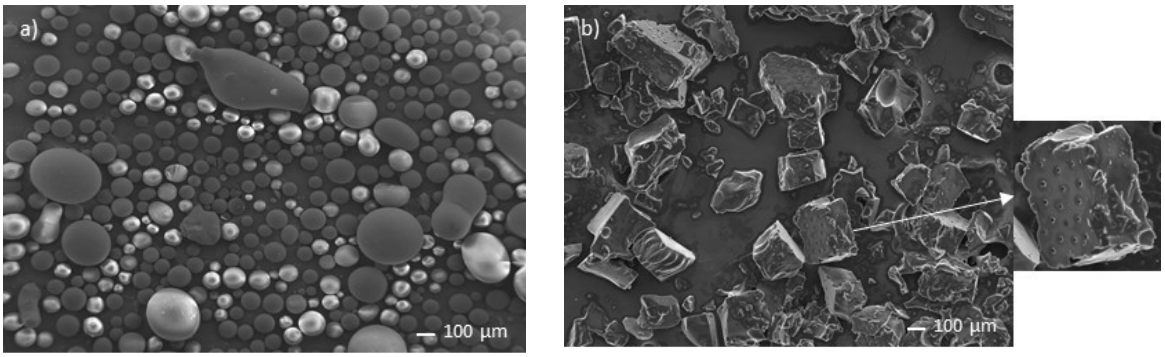

Figure 11 Surface Scanning Electron Micrograph (SEM) images of a) template PMMA spheres with 50x magnification. b) Surface SEM images of 1@PMMA with 100x magnification showing microporous morphology.

A side paragraph should be devoted to the emission profile of the $^5D_4 \rightarrow {}^7F_5$ transition band of the Tb^{III} complex when exposed to a gradual increase of temperature. The $^5D_4 \rightarrow {}^7F_6$ transition is a magnetic-dipole and its intensity does not depend on the coordination environment. In contrast, the $^5D_4 \rightarrow {}^7F_5$ transition, because of its electric character, depends strongly on the ligand field around the Tb^{III} centre.

The $^5D_4 \rightarrow {}^7F_5$ transition band of **1** is split into four 'shoulders' with different energy levels at 545, 547, 551 and 554 nm. Similar to what was reported for the Eu^{III} analogue,[41] under heating $[C_2mim][Tb(fod)_4]$ undergoes a reasonable increase of the intensity in the second most intense sublevel that comprise the $^5D_4 \rightarrow {}^7F_5$ transition.

The emission spectra profile changes during heating, suggesting modification of the chemical environment around Tb^{III}, allows its categorization as a single-centered emission thermal probe.

Pioneer work developed by Yuasa and Kawai uses the idea that a significant increment in emission intensity at 616 nm (shoulder) for Eu^{III}, relative to the emission at 613 nm, is directly related to the temperature of exposure.[42] The emission intensity at 545 nm decreases linearly as the temperature is increased from 25 to 40 °C. Conversely, the emission intensity at 548 nm increases with an increase of temperature. Above 40 ºC and up to 75 ºC, this ratio remains almost constant due to the very low intensity of the emission band, with flattening of the band shoulders (Figure 12a and 12b). It is important to note that the fod^- ligand has several strong electron withdrawing groups ($–CF_3$) that increase the ionic degree of the ligand. The consequence is a stronger interaction with the metal, which induces higher Lewis acidity character to the lanthanide ion.

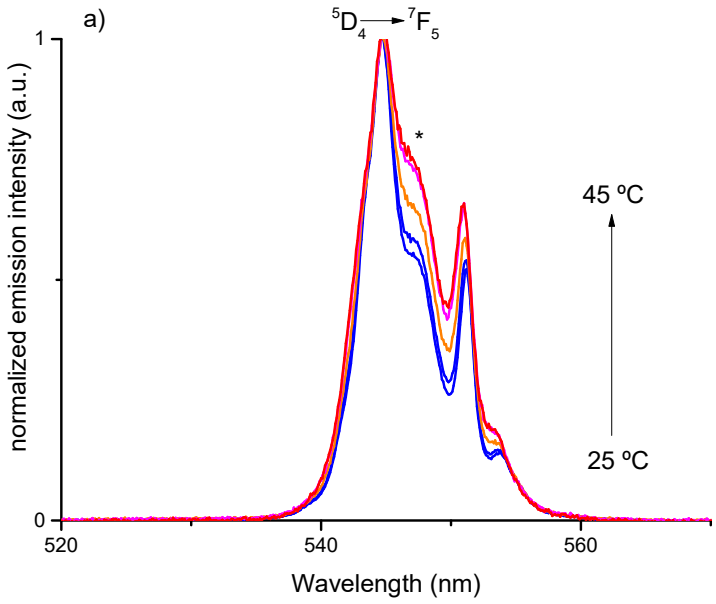

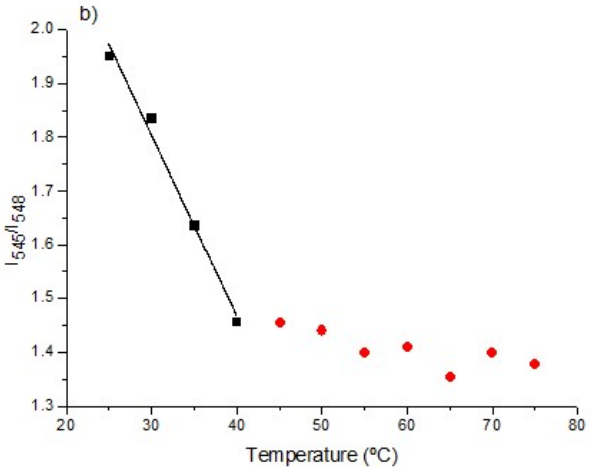

Figure 12 a) Emission spectra between 520 nm and 570 nm of $[C_2mim][Tb(fod)_4]$ in the solid state upon excitation at 340 nm. b) Δ=-0.0337T+ 2.81 (R^2=0.994) * emission band at 548 nm.

Crystallographic studies

The crystallographic studies of $[C_2mim][Tb(fod)_4]$ did not allow us to fully elucidate the crystal structure. Even high-quality SCXRD data (obtained from several crystals from different batches) proved to be very challenging due to at least two factors – heavy disorder of the fod ligands around the metal centres and the microstructure of the crystals. All crystals were found to delaminate easily when minor external pressure was applied along a specific direction as a possible consequence of a weak connectivity between the fluorine-containing groups. This is in line with the frequently observed segregation of the $-CF_3$ groups in Tf_2N salts. Nonetheless, we were able to reach some important conclusions.

$[C_2mim][Tb(fod)_4]$ crystallizes in the orthorhombic space group Pna21 (#33) with the following unit cell parameters a = 44.30 Å, b = 10.35 Å and c = 25.94 Å showing negligible variation for all tested crystals from different batches.

The asymmetric unit contains two $[C_2mim]^+$ cations and two discrete anionic $[Tb(fod)_4]^-$ complexes, with each terbium cation coordinated to four highly disordered fod^- linkers to give a relatively ordered $\{TbO_8\}$ square antiprismatic coordination sphere, as depicted in Figure S5 (please note: though the linkers were found to be disordered, the coordinating oxygen atoms were modelled at fixed positions with no apparent structural disorder) Some solvent molecules are probably present in what otherwise would be voids in the structure. The disordered fod^- linkers occupy at least four different positions. The analysis of the O···O distances revealed two interesting aspects – they are a few % shorter in the planes normal to the local pseudo-21 axis compared with those along the axis and they show no clear segregation in these planes. This suggests that the fod^- disorder may be crystallographically limited to the 180º rotation of the carbon chain around the same two coordinated O positions plus 90º rotation involving of the neighbouring O positions (totally four in-plane options).

Conclusions

Lanthanide-based thermometers are essentially dual-center, based on the Tb^{III} and Eu^{III} emission intensity ratio: $^5D_4 \rightarrow {}^7F_5$ (Tb^{III}) and $^5D_0 \rightarrow {}^7F_2$ (Eu^{III}).

The advantage of this new molecular temperature sensor is the use of an extremely low amount of Eu^{III} complex, which allows naked-eye detection of discrete temperature changes around ambient temperatures.

We were able to identify three different linear thermometric regimes for the $[C_2mim][Tb(fod)_4]_{0.99985}.[C_2mim][Tb(fod)_4]_{0.00015}$ complex mixture, with very different and relevant relative sensitivities. This molecular temperature sensor is highly sensitive over the physiological temperature range (35-45 ºC) with a relative sensitivity of 5.5% C^{-1} at 36 ºC.

We predict that fine-tuning the Tb^{III}/Eu^{III} mixture by doping with slightly higher concentrations of Eu^{III} complex will yield very interesting results in the 0-25 ºC range, which foresees important applications at an industrial level.

A semi-transparent luminescent film of PMMA was successfully prepared by incorporation of 10% of the studied Tb/Eu complex mixture. Notably, this molecular plastic material presented a two-fold increase in the luminescent quantum yield compared with the lanthanide complex mixture. More interesting is the observed thermochromism: a small variation of only 5 ºC, from 25 to 30 ºC, allows the colours emitted by the functionalized material to change from green to yellow and then to a white tone at only 35 ºC. Finally, at temperatures higher than 55 ºC the red emission from Eu^{III} dominates with different tones of red/pink until 70 ºC. This optically active film foresees interesting applications in photovoltaic science. Future research demands the evaluation of these films in the co-sensitization of Dye Sensitized Solar Cells as a means of extending the light harvesting efficiency.

Experimental Section

General

Reagent grade chemicals were obtained from Aldrich and used without further purification.

Microanalyses for C and H were carried out using a Thermo Finnigan-CE Instruments Flash EA 1112 CHNS series. FT-IR spectra (range 4000– 400 cm@1) were collected as KBr pellets (Sigma-Aldrich, FT-IR grade) using a Thermo Scientific Nicolet iS50 FT-IR spectrometer, by averaging 64 scans at a maximum resolution of 4 cm@1. Analysis of

the heated sample was performed by heating initially **1** in an oven and then preparing the KBr pellet, ensuring that the pellet had a purple colour during acquisition of the FT-IR spectra. TGA curves were obtained using a Thermal Analysis Ta Q500-2207, with a scanning rate of 10 °C min^{-1} for 1, with samples weighing around 8 mg in aluminium crucibles. The calibration of the TGA equipment was made by following the recommendation described in the manufacturer's manual.

Luminescence spectra were measured by using a SPEX Fluorolog-3 Model FL3-22 spectrofluorimeter, with 0.5 nm slits and a measurement step of 0.1 nm. The excitation wavelength was 350 nm.

Luminescence quantum efficiencies were measured by the absolute method with an Integrated Sphere.[43] All spectra are corrected with correction functions provided by the supplier by following standard procedures.

Lifetime measurements were carried out in a Jobin Yvon FluoroLog fluorescence spectrometer with a pulsed xenon lamp with full-width at half-maximum of 3 μs. Decays were collected with an integration time of 250 μs and with increasing delays, with an initial delay of 50 μs to remove any interference from the lamp. Temperatures were kept constant during measurements using a Wavelength Electronics LFI-3751 Thermoelectric Temperature Controller, with a minimum 1 min K^{-1} waiting time during heating ramps.

Emission decays were obtained with spectral resolution of 5 nm, with a perpendicular geometry relative to the laser excitation, using 50 lamp pulses for each delay. Luminescence decay traces at each wavelength were analysed using least-squares fittings of the experimental data, using Solver from Microsoft Excel.

The luminescence of 1@PMMA with increasing temperature was monitored using an optical fiber focusing on a small amount of sample while heating over a thermostatic heating plate (Argolab).[41] The temperature range was from 25 to 100 °C.

The mass spectra were acquired on a LCQ Fleet ion trap mass spectrometer equipped with an ESI ion source (Thermo Scientific TM) operated in the ESI positive and negative ion modes and using the following optimized parameters: ion spray voltage, 4.5 kV; capillary voltage, 16/@18 V; tube lens offset, @70/58 V; sheath gas (N_2), 40 arbitrary units; auxiliary gas (N_2), 20 arbitrary units; capillary temperature, 300 °C. Spectra typically correspond with the average of 20–35 scans and were recorded in the range 70–1500 Da. Data acquisition and data processing were done with Thermo Xcalibur 2.3 software.

Several plate-like crystals were inspected and isolated using a Stemi 2000 stereomicroscope equipped with Carl Zeiss lenses. This allowed the identification of large colourless plates which were investigated using single-crystal X-ray diffraction. Crystals were selected manually and harvested from the batch samples and mounted on glass fibers. Preliminary X-ray diffraction data were collected at 160(2) K on an Oxford Diffraction SuperNova, dual radiation diffractometer using a Cu Kα microsource tube (λ = 1.540598 Å), an Atlas CCD detector, and an Oxford Instruments Cryostream XL Series low temperature device.

Synthetic procedures

The solid white complex was prepared according to a previously reported procedure adequately adapted for the correspondent terbium analogue.[41]

$[C_2mim][Tb(fod)_4]$: 4.1 eq. of NaOH (0.176 g, 2.196 mmol, 50% w/w aqueous solution) were added to an ethanol solution of 4.1 eq. of Hfod (0.650 g, 2.196 mmol) and left stirring for 2 h. 1 eq. of $TbCl_3 \cdot 6H_2O$ (0.200 g, 0.536 mmol) was then added to the reaction mixture and the resulting solution left stirring for 2 h followed by the addition 1 eq. of 1-

ethyl-3-methylimidazolium tetrafluoroborate ($EMIMBF_4$, 0.110 g, 0.558 mmol). After 1 h the solvent was removed under low pressure and the resulting solid was extracted with CH_2Cl_2. NaCl was removed by filtration and the pure compound was recovered as a white powder after solvent evaporation, at ambient temperature with a yield of *ca*. 80 %. Anal. Calcd. for $[C_6H_{11}N_2][Tb(C_{10}H_{10}O_2F_7)_4]$: C, 38.08; H, 3.54; N, 1.93%. Experimental; C, 38.26; H, 3.66; N, 1.80%.

ESI/MS: m/z 1339.1 $[Tb(C_{10}H_{10}O_2F_7)_4]^+$ (Figure S2)

The FTIR spectrum of $[C_2mim][Tb(fod)_4]$ at 20 ºC presents a broad band around 3420 cm^{-1}, absent after heating at 150°C, characteristic of the bending vibrations of H–O–H from the water adsorbed in the tablet during preparation (Figures S3 and S4). Medium intensity bands appear in the ranges 3000-3200 cm^{-1} and 2860-3000 cm^{-1} and are ascribed to the symmetric and asymmetric stretching vibrational modes of the C-H bonds in the alkyl groups of the ligand (fod^-) and counter-ion (C_2mim), respectively. The very strong band around 1628 cm^{-1} is due to the C-O bonds, the band at 1575 cm^{-1} is assigned to the –C–O stretching mode of the fod^- ligands and the band at 1509 cm^{-1} is typical of the alkene C-C bonds. The bands in the ranges 600–1200 cm^{-1} and 800–970 cm^{-1} are due to the stretching modes of the C–C and C–F bonds, respectively. Similar observations were obtained with the Eu analogue, $[C_2mim][Eu(fod)_4]$;[24] heating does not affect the infrared profile of the $[C_2mim][Tb(fod)_4]$, but unlike the former, there is no discernible broadening of the peaks associated with increased motion of adjacent atoms, which might indicate a more rigid structure (Figure S3).

$[C_2mim][Tb(fod)_4]_{0.99985}$:$[C_2mim][Eu(fod)_4]_{0.00015}$) (**1**) Solutions of $[C_2mim][Tb(fod)_4]$ and $[C_2mim][Eu(fod)_4]$ in CH_2Cl_2 were mixed according in the studied Tb^{III}/Eu^{III} ratio (0.99985:0.00015). The solvent was removed under reduced pressure. The homogeneity

of the mixture of complexes was confirmed by analysis of the emission spectra at different points within the powder.

1@PMMA: 10% (w/w) of **1** was dissolved in CH_2Cl_2 and added to a solution of PMMA in tetrahydrofuran. The resulting homogeneous solution was spread on a glass Petri dish and the solvent was allowed to evaporate slowly.[44] Attempts to remove the film from the glass were unsuccessful due to the brittle character of the material.

Both solid complexes and 1@PMMA presented stability for several months and as suspensions under very weak basic and acid conditions.

The FTIR spectrum of 1@PMMA at 20 ºC and 150 ºC presents the same vibration bands, although with different intensities (Figure S4).

The crystal structure of $[C_2mim][Tb(fod)_4]$ was tentatively solved using the dual space algorithm implemented in SHELXT-2014, which allowed the immediate location of all of the heaviest atoms composing the coordination sphere of the complexes. Due to the high level of disorder of the fod^- linkers, the remaining modelling and refinement of the two complexes present in the asymmetric unit was impossible. The obtained results are presented in the supplementary information file, including a schematic representation of the molecule (Figure S5).

Acknowledgement

This work was supported by the Associated Laboratory for Sustainable Chemistry-Clean Processes and Technologies- LAQV, which is financed by national funds from FCT/MEC (UID/QUI/50006/2019) and co-financed by the ERDF under the PT2020 Partnership Agreement (POCI-01-0145-FEDER – 007265). This work was partially developed within the scope of the project CICECO-Aveiro Institute of Materials, UIDB/50011/2020 &

UIDP/50011/2020, financed by national funds through the FCT/MEC and when appropriate co-financed by FEDER under the PT2020 Partnership Agreement. The NMR spectrometers are part of The National NMR Facility, supported by Fundação para a Ciência e a Tecnologia (RECI/BBB-BQB/0230/2012). This work was also supported by Fundação para a Ciência e a Tecnologia (FCT) through the projects UIDB/00100/2020, and by Fundação para a Ciência e a Tecnologia through the contract nº IST-ID/077/2018 (Bernardo Monteiro). Cláudia C. L. Pereira thanks Fundação para a Ciência e a Tecnologia, MCTES, for the Norma transitória DL 57/2016 Program Contract. J. A. acknowledges Fundação para a Ciência e a Tecnologia (FCT, I.P.) for funding under grant SFRH/BPD/120599/2016 and project PTDC/QUI-QFI/32007/2017. This work was developed within the scope of the project CICECO-Aveiro Institute of Materials, UIDB/50011/2020 & UIDP/50011/2020, financed by national funds through the FCT/MEC and when appropriate co-financed by FEDER under the PT2020 Partnership Agreement. RFM gratefully acknowledges FCT for a Junior Research Position (CEECIND/00553/2017).

References

[1] M.W. Dewhirst, Z. Vujaskovic, E. Jones, D. Thrall; Re-setting the biologic rationale for thermal therapy, *Int. J. Hyperthermia* **2005**, 21, 779–790.

[2] A. Bakker, R. Holman, D. B. Rodrigues, H. D. Trefná, P. R. Stauffer, G. Van Tienhoven; Analysis of clinical data to determine the minimum number of sensors

required for adequate skin temperature monitoring of superficial hyperthermia treatments, *Int. J. Hyperth.* **2018**, 34, 910–917.

[3] F. V. Bussche, A. M. Kaczmarek, J. Schmidt, C. V. Stevens, P. Van Der Voort; Lanthanide grafted phenanthroline-polymer for physiological temperature range sensing, *J. Mater. Chem. C* **2019**, 7, 10972-10980.

[4] L. B. Guimarães, A. M. P. Botas, M. C. F. C. Felinto, R. A. S. Ferreira, L. D. Carlos, O. L. Malta, H. F. Brito; Highly sensitive and precise optical temperature sensors based on new luminescent Tb^{3+}/Eu^{3+} tetrakis complexes with imidazolic counterions, *Mater. Adv.* **2020**, 1, 1988-1995.

[5] T. Xia, Z. Shao, X. Yan, M. Liu, L. Yu, Y. Wan, D. Chang, J. Zhang, D. Zhao; Tailoring the triplet level of isomorphic Eu/Tb mixed MOFs for sensitive temperature sensing, *Chem. Commun.* **2021**, 57, 3143–3146.

[6] Y. Zhou, B. Yan, F. Lei; Postsynthetic lanthanide functionalization of nanosized metal–organic frameworks for highly sensitive ratiometric luminescent thermometry*Chem. Commun.* **2014**, 50, 15235-15238.

[7] C. Gu, Y. Ding, X. Quan, M. Gong, J. Yu, D. Zhao, C. X. Li; Near-infrared luminescent Nd^{3+}/Yb^{3+}-codoped metal–organic framework for ratiometric temperature sensing in physiological range, *J. Rare Earth*, **2021**, 39, 1024-1030.

[8] D. Ananias, C. M. Mongis, L. D. Carlos, João Rocha; Cryogenic Luminescent Ratiometric Thermometers Based on Tetragonal Na[LnSiO4]·xNaOH (Ln = Gd, Tb, Eu; x ≈ 0.2), *Eur. J. Inorg. Chem.* **2020**, 1852–1859.

[9] A. M. Kaczmarek, Y-Y. Liu, M. K. Kaczmarek, H. Liu, F. Artizzu, L. D. Carlos, P. Van Der Voort; Developing Luminescent Ratiometric Thermometers Based on a Covalent Organic Framework (COF), *Angew. Chem. Int. Ed.* **2020**, 59, 1932 – 1940.

[10] G.E. Khalil, K. Lau, G. D. Phelan, B. Carlson, M. Gouterman, J. B. Callis, L. R. Dalton, Europium beta-diketonate temperature sensors: Effects of ligands, matrix, and concentration, *Rev. Sci. Instrum.* **2004**, 75, 192-206.

[11] A. Bednarkiewicz, L. Marciniak, L. D. Carlos, D. Jaque; Standardizing luminescence nanothermometry for biomedical applications, *Nanoscale* **2020**, 12, 14405–14421.

[12] B. Monteiro, M. Outis, H. Cruz, J. P. Leal, C. A. T. Laia, C. C. L. Pereira; A thermochromic europium(III) room temperature ionic liquid with thermally activated anion–cation interactions, *Chem. Commun.* **2017**, 53, 850–853.

[13] S. A. Bhat, K. Iftikhar; Optical Properties of New Terbium(III) Ternary Complexes Containing Anionic 6,6,7,7,8,8,8-heptafluoro-2,2-dimethyl-3,5-octanedione and Neutral Sensitizers in Solution, Solid and PMMA Thin Films: Intra and Interphase Colour Tuning, *Photochem. Photobiol*. **2021**, 97, 688-699.

[14] K. P. Zhuravlev, V. I. Tsaryuk, V. A. Kudryashova; Photoluminescence of europium and terbium trifluoroacetylacetonates. Participation of LMCT state in processes of the energy transfer to Eu^{3+} ion, *J. Fluor. Chem.* **2018**, 212, 137-143.

[15] Z. Ahmed, K. Iftikhar; Efficient Layers of Emitting Ternary Lanthanide Complexes for Fabricating Red, Green, and Yellow OLEDs, *Inorg. Chem.* **2015**, 54, 11209–11225.

[16] Y-J. Huang, C. Ke, L-M. Fu, Y. Li, S-F. Wang, Y-C. Ma, J-P. Zhang, Y. Wang; Excitation Energy-Transfer Processes in the Sensitization Luminescence of Europium in a Highly Luminescent Complex, *ChemistryOpen* **2019**, 8, 388– 392.

[17] S. Hamada, Y. Funasako, T. Mochida, D. Kuwahara, K. Yoza; Phase transitions and thermal properties of decamethylferrocenium salts with perfluoroalkyl-sulfonate and -carboxylate anions exhibiting disorder, *J. Organomet. Chem.* **2012**, 713, 35– 41.

[18] T. Mochida, Y. Funasako, M. Ishida, S. Saruta, T. Kosone, T. Kitazawa; Crystal Structures and Phase Sequences of Metallocenium Salts with Fluorinated Anions: Effects of Molecular Size and Symmetry on Phase Transitions to Ionic Plastic Crystals, *Chem. Eur. J.* **2016**, 22, 15725– 15732.

[19] S. Dasari, S. Singh, S. Sivakumar, A. K. Patra; Dual-Sensitized Luminescent Europium(III) and Terbium(III) Complexes as Biomaging and Light-Responsive Therapeutic Agents, *Chem. Eur. J.* **2016**, 22, 17387-17396.

[20] U. Cho, J. K. Chen; Lanthanide-Based Optical Probes of Biological Systems, *Cell Chem. Biol.*, **2020**, 27, 921-936.

[21] J. J. Freeman, G. A. Crosby; Spectra and Decay Times of the Luminescences observed from Chelated Rare Earths ions, *J. Phys. Chem.* **1963**, 67, 2717-2723.

[22] G. A. Crosby, R. E. Whan, J. J. Freeman; Spectroscopic Studies of rare Earth Chelates*, Phys. Chem.* **1962**, 66, 2493-2499.

[23] L. S. Villata, E. Wolcan, M. R. Félix, A. L. Capparell; Solvent quenching of the $^5D_0 \rightarrow {}^7F_2$ emission of Eu(6,6,7,7,8,8,8-heptafluoro-2,2-dimethyl-3,5-octanedionate)$_3$, *J. Photochem. Photobiol. A: Chemistry* **1998**, 115, 185-189.

[24] M. Outis, J. P. Leal, J. Avó, B. Monteiro, C. C. L. Pereira; A Europium(III) Complex Embedded in a Polysulfone Host Matrix: A Flexible Film with Temperature-Responsive Ratiometric Behaviour, *ChemPlusChem* **2020**, 85, 2629–2635.

[25] S. M. Borisov, I. Klimant; Blue LED excitable temperature sensors based on a new europium(III) chelate, *J. Fluoresc.* **2008**, 18, 581-589.

[26] J. Yu, L. Sun, H. Pengac, M. I. J. Stich; Luminescent terbium and europium probes for lifetime based sensing of temperature between 0 and 70 °C, *J. Mater. Chem.* **2010**, 20, 6975–6981.

[27] G. E. Khalil, K. Lau, G. D. Phelan, B. Carlson, M. Gouterman, J. B. Callis, L. R. Dalton; Europium beta-diketonate temperature sensors: Effects of ligands, matrix, and concentration, *Re*V. *Sci. Instrum*. **2004**, *75*, 192.

[28] R. Ilmi, K. Iftikhar; Optical emission studies of new europium and terbium dinuclear complexes with trifluoroacetylacetone and bridging bipyrimidine. Fast radiation and high emission quantum yield, *Polyhedron* **2015**, 102, 16-26.

[29] A. Fratini, G. Richards, E. Larder, S. Swavey; Neodymium, Gadolinium, and Terbium Complexes Containing Hexafluoroacetylacetonate and 2,2‘-Bipyrimidine: Structural and Spectroscopic Characterization, *Inorg. Chem.* **2008**, 47, 1030-1036.

[30] C. D. S. Brites, S. Balabhadra and L. D. Carlos; Lanthanide-Based Thermometers: At the Cutting-Edge of Luminescence Thermometry, *Adv. Opt.Mater.* **2018**, 7, 1801239.

[31] D. Maraab, F. Artizzua, B. Laforcec, L. Vinczec, K. Van Heckeb, R. Van Deuna, A. M. Kaczmarek; Novel tetrakis lanthanide β-diketonate complexes: structural study, luminescence properties and temperature sensing, *J. Lumin.* **2019**, 213, 343-355.

[32] D. Ananias, A. D. G. Firmino, R. F. Mendes, F. A. A. Paz, M. Nolasco, L.D. Carlos, J. Rocha; Excimer Formation in a Terbium Metal–Organic Framework Assists Luminescence Thermometry, *Chem. Mater.* **2017**, 29, 9547-9554.

[33] D. Mara, A. M. Kaczmarek, F. Artizzu, A. Abalymov, A. G. Skirtach, K. Van Hecke, R. Van Deun; Luminescent PMMA Films and PMMA@SiO_2 Nanoparticles with Embedded Ln^{3+} Complexes for Highly Sensitive Optical Thermometers in the Physiological Temperature Range, *Chem. Eur. J.* **2021**, 27, 6479-6488.

[34] M. B. Vialtsev, A. I. Dalinger, E. V. Latipov, L. S. Lepnev, S. E. Kushnir, S. Z. Vatsadze, V. V. Utochnikova; New approach to increase the sensitivity of Tb–Eu-based luminescent thermometer, *Phys. Chem. Chem. Phys.* **2020**, 22, 25450-25454.

[35] Y. Yang, Y. Wang,Y. Feng, X. Song, C. Cao, G. Zhang, W. Liu; Three isostructural Eu^{3+}/Tb^{3+} co-doped MOFs for wide-range ratiometric temperature sensing, *Talanta* **2020**, 208, 120354.

[36] D. L. Dexter; A Theory of Sensitized Luminescence in Solids, *J. Chem. Phys.* **1953**, 21, 836–850.

[37] N. M. Shavaleev, G. Accorsi, D. Virgil, Z. R. Bell, T. Lazarides, G. Calogero, N.

Armaroli, M. D. Ward; Syntheses and Crystal Structures of Dinuclear Complexes Containing d-Block and f-Block Luminophores. Sensitization of NIR Luminescence from Yb(III), Nd(III), and Er(III) Centers by Energy Transfer from Re(I)− and Pt(II)−Bipyrimidine Metal Centers, *Inorg. Chem.* 2005, 44, 61-72.

[38] P. Miluski, M. Kochanowicz, J. Zmojda, T. Ragin, D. Dorosz; Spectroscopic investigation of $Tb(tmhd)_3$-$Eu(tmhd)_3$ co-doped poly(methyl methacrylate) fibre, *Opt. Mater.* **2019**, 87, 112-116.

[39] S. Sivakumar, M. L. P. Reddy; Bright green luminescent molecular terbium plastic materials derived from 3,5-bis(perfluorobenzyloxy)benzoate, *J. Mater. Chem.* **2012**, 22, 10852–10859.

[40] M.A. Cardoso, S.F.H. Correia, A.R. Frias, H. M. R. Gonçalves, R. F. P. Pereira, S. C. Nunes, M. Armand, P. S. Andre, V. de Zea Bermudez, R. A. S. Ferreira; Solar spectral conversion based on plastic films of lanthanide-doped ionosilicas for photovoltaics: Down-shifting layers and luminescent solar concentrators, *J. Rare Earth* **2020**, 38, 531-538.

[41] M. Outis, J. P. Leal, M. H. Casimiro, B. Monteiro, C. C. L. Pereira; Thermochromism of Highly Luminescent Photopolymer Flexible Films Based on Eu (III) Salts Confined in Polysulfone, *Materials* **2020**, 5394.

[42] J. Yuasa, R. Mukai, Y. Hasegawa, T. Kawai; Ratiometric luminescence thermometry based on crystal-field alternation at the extremely narrow $^5D_0 \rightarrow {}^7F_2$ transition band of europium(III), *Chem. Commun.* **2014**, 50, 7937-7940.

[43] M. S. Wrighton, D.S. Ginley, D. L. Morse; Technique for the determination of absolute emission quantum yields of powdered samples, *J. Phys. Chem.* 1974, 78, 2229-2233.

[44] K. Lunstroot, K. Driesen, P. Nockemann, L. Viau, P. H. Mutin, A. Vioux, K. Binnemans; Ionic liquid as plasticizer for europium(iii)-doped luminescent poly(methyl methacrylate) films, *Phys. Chem. Chem. Phys.* **2010**, 12, 1879–1885.